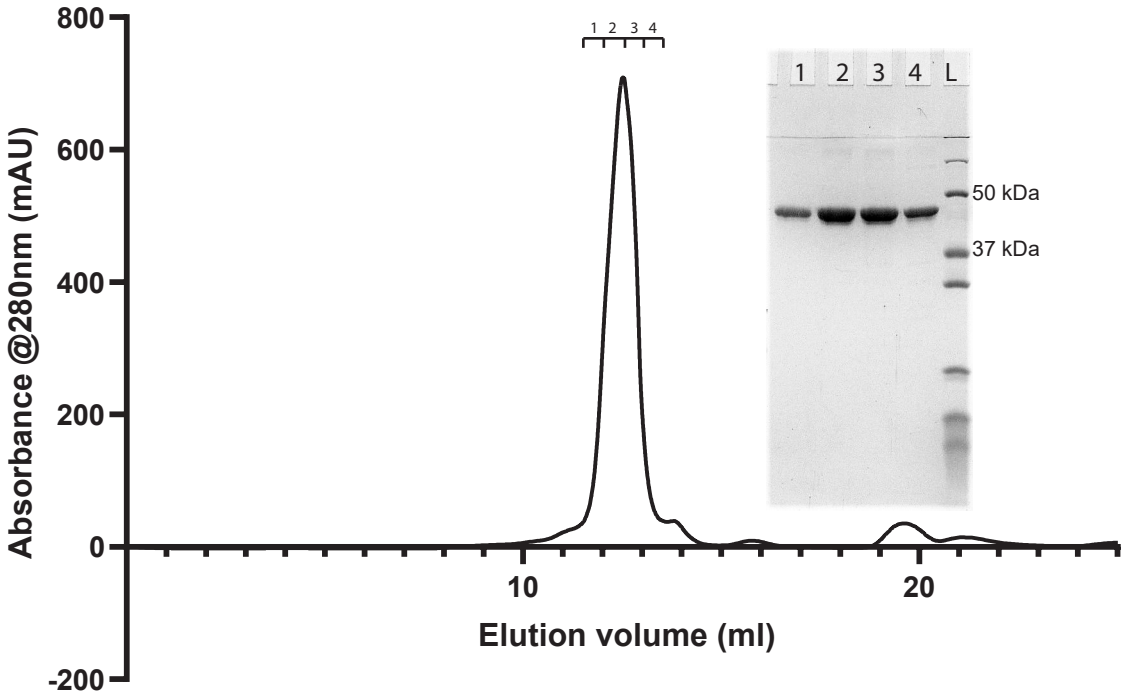

Figure S1. Size exclusion chromatography purification profile of NorC. NorC elutes in a single homogeous monomeric population (collected fractions labelled at the top of the elution peak), with SDS gel profile of the fractions collected shown in inset. L = Ladder.

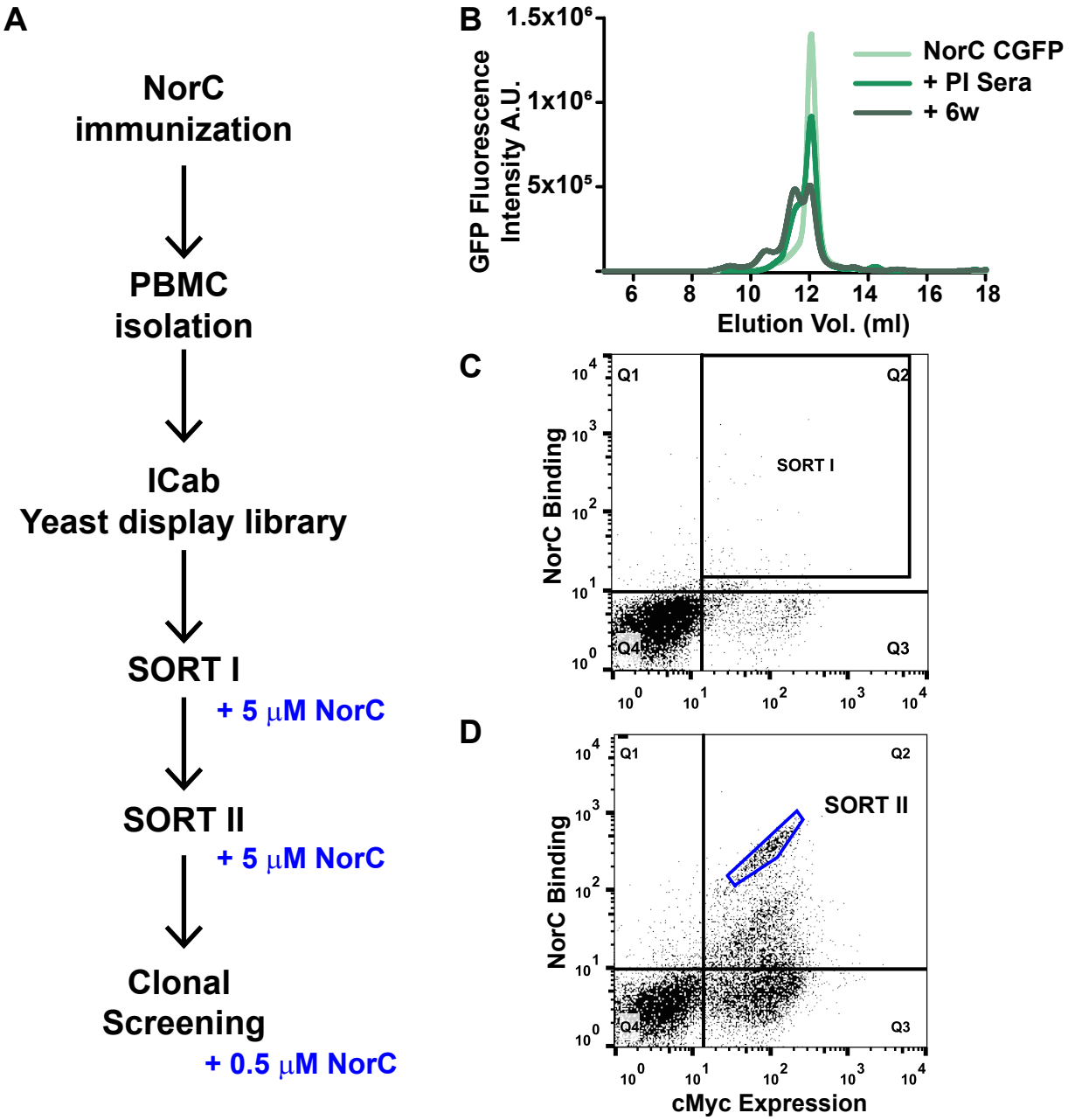

Figure S2. **A**, Flowchart of screening process adopted for identifcation of binders against NorC. PBMCs isolated from camels immunized against NorC were used to isolate ICabs (VHH), which were cloned into pPNL6 yeast display vector to build the library. FACS based screening was done through two steps of sorting. Individual clones after sort II were independently screened against NorC. **B**, FSEC of NorC-CGFP performed with preimmune sera and sera after 6 weeks of immunization. Immunized sera displays clear shift of NorC towards a higher molecular weight. **C**, First sorting step after library construction. Cells isolated from the gate drawn in Q2 were used for enrichment. **D**, Second sorting step yielded a sub-population with prominent shifts in binding and expression (blue gate).

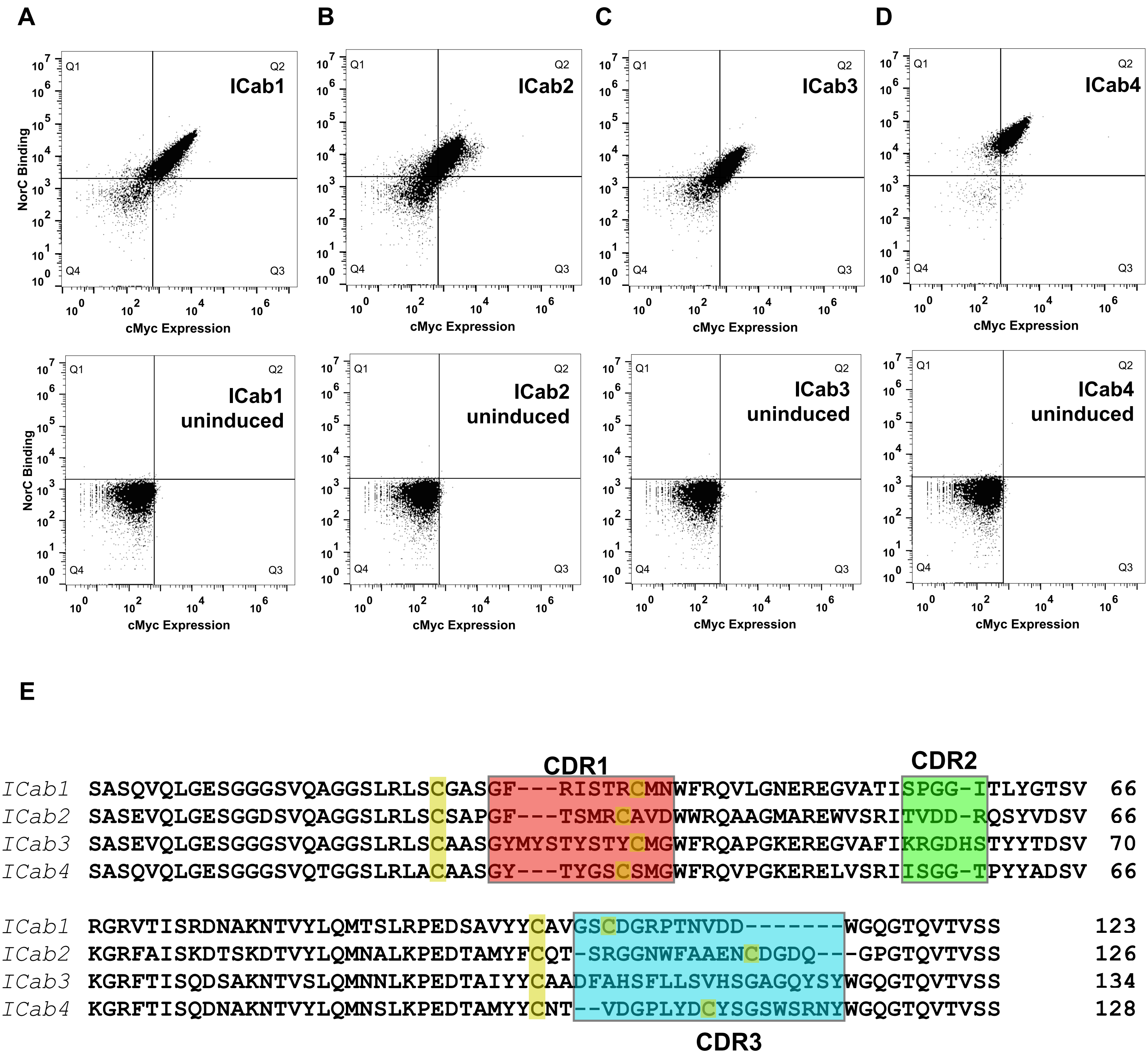

Figure S3. **A-D**, FACS analyses of individual clones ICabs 1-4, double labeled to analyze both NorC binding and surface expression using cMyc tag. Panel C is also a part of Fig. 1A and B. Uninduced controls for each of the clones is depicted in the bottom panels. **E**, Sequence alignment of unique ICabs 1-4 identified in the screening process. ICab3 was chosen for further analyses in this study.

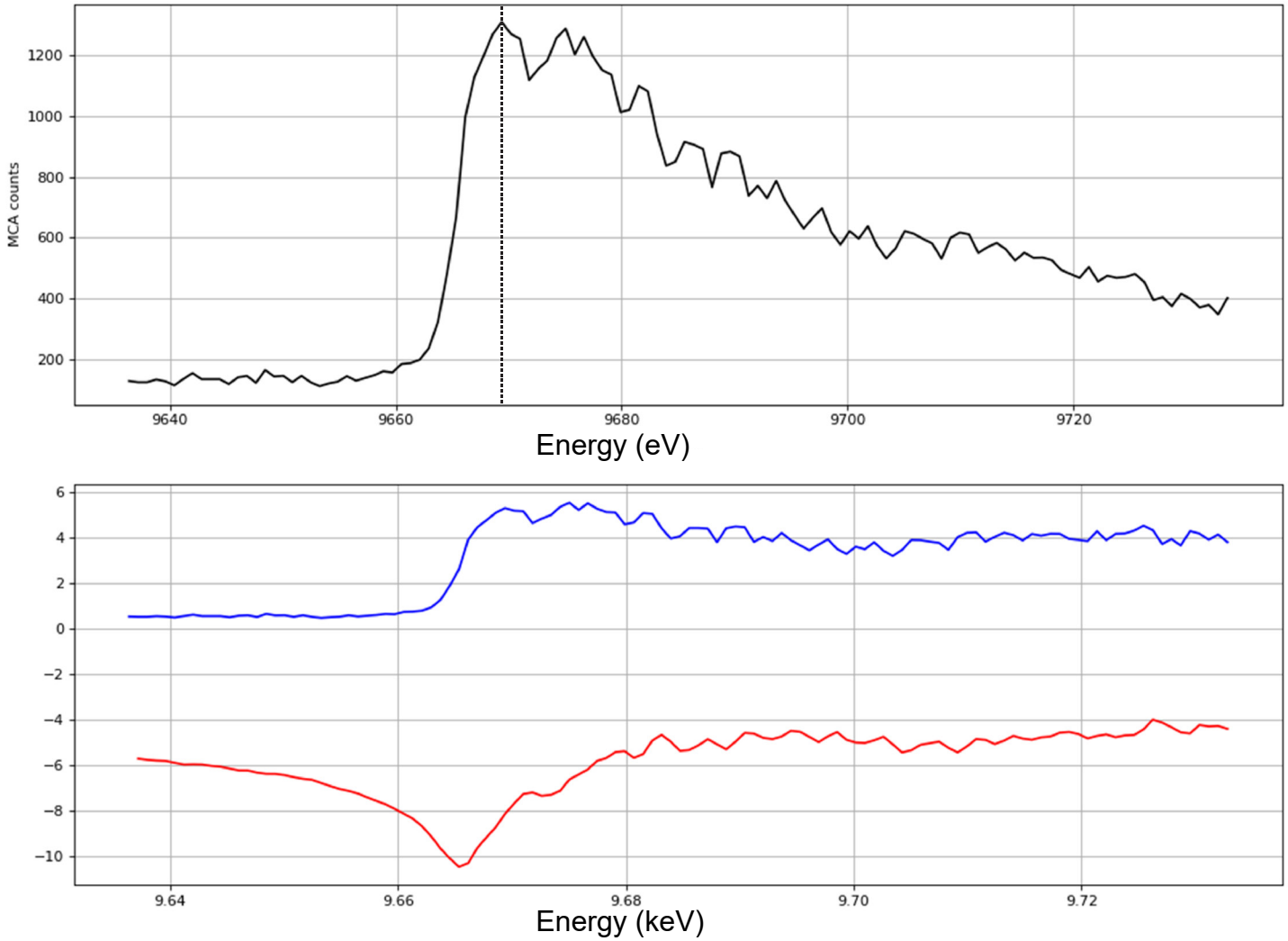

Energy (keV)	f’	f’’
9.67504	-6.62	5.51
9.66534	-10.45	2.59

Figure S4. X-ray energy scan of ICab3 crystal showing absorption edge corresponding to Zn atom.

A

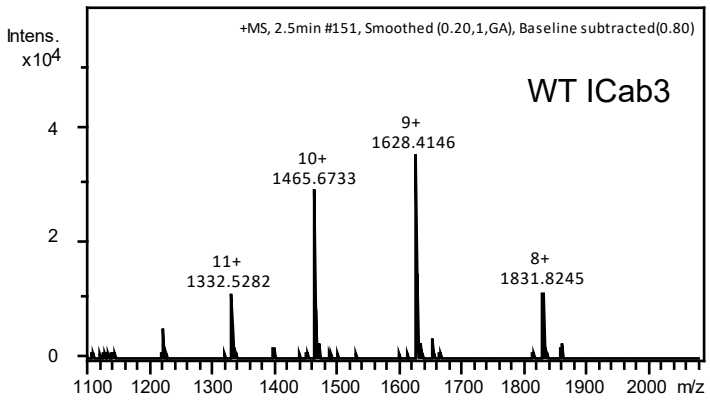

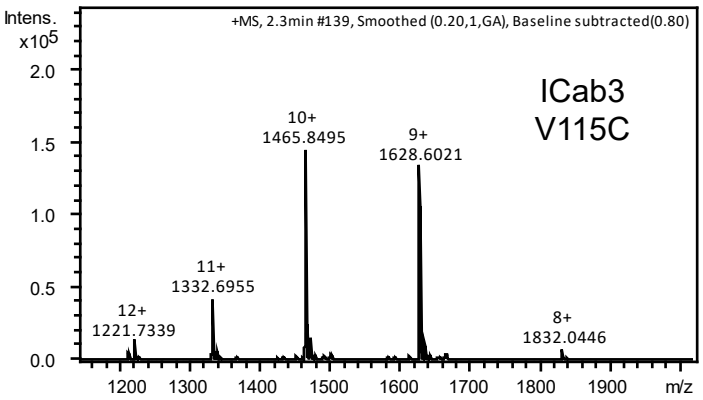

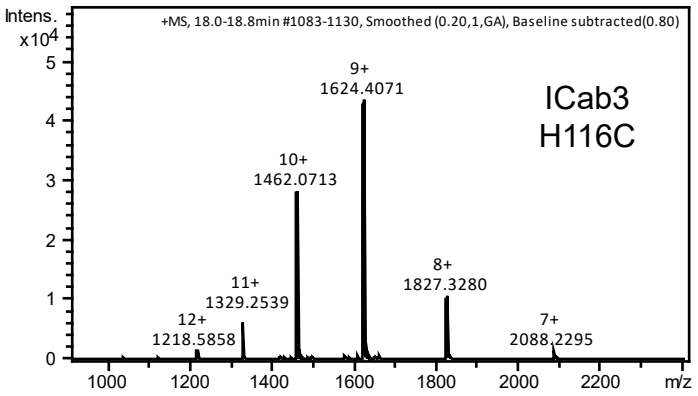

Mol. mass (Da)	WT ICab3	ICab3 V115C	ICab3 H116C
Expected*	14649.14	14653.15	14615.14
Observed	14646.72	14648.55	14610.74
Δmass	2.42	4.60	4.40

*Expected mass corresponds to a species with all cysteines in reduced state.

B

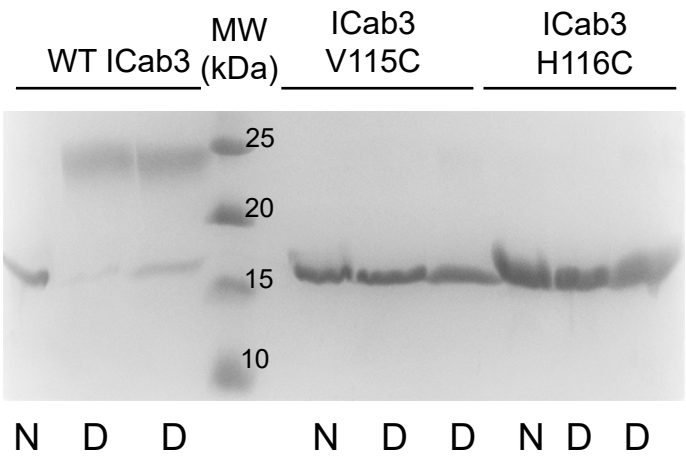

Figure S5. Investigation into the nature of cysteines in ICab3 and its mutants. **A**, ESI mass spectrometry determined WT ICab3's mass as a Zn-free species with two oxidised cysteines. The observed masses of both the mutants corresponded to species harboring all 4 cysteines in oxidized state, with Cys115/Cys116 forming a disulfide with Cys40. **B**, PEG-Maleimide crosslinking assay was done with ~0.5mg/ml of protein and 20x molar excess of PEG(5000)-maleimide. N: native protein set up for crosslinking; D: heat denaturation of protein at 90°C for 10 minutes in presence of 0.5% SDS done prior to setting up crosslinking assay. While WT ICab3 formed 1 molecule adduct with PEG-Maleimide in denaturing condition, neither of the mutants could crosslink with PEG-Maleimide.

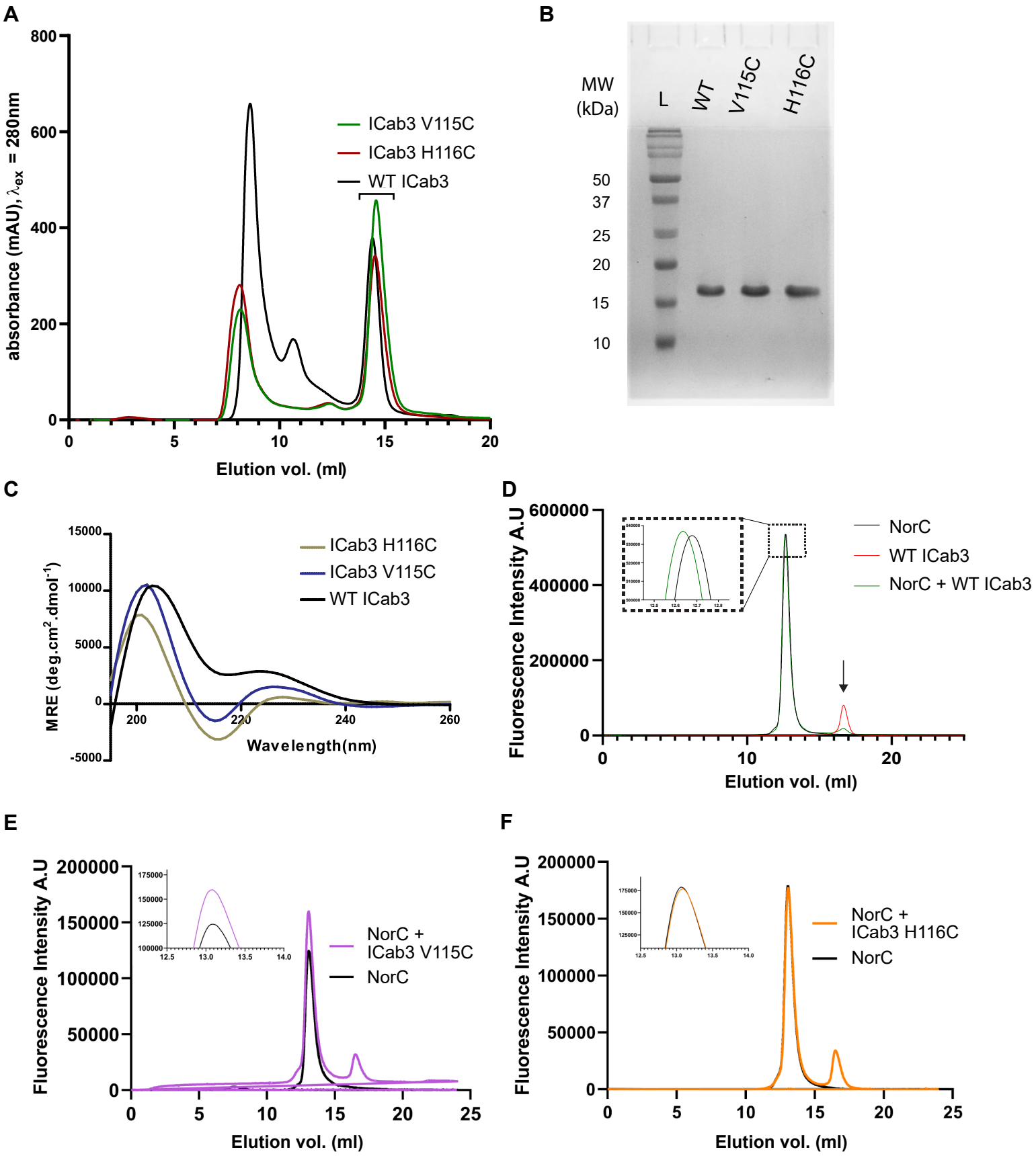

Figure S6. **A,** Size exclusion chromatography profiles of WT ICab3 and its mutants ICab3 V115C and ICab3 H116C. **B**, SDS-PAGE image of SEC purified peaks of WT ICab3 and its mutants, with their circular dichroism profiles in panel **C**. Fluorescence-detection size exclusion chromatography profiles of NorC incubated with (**D**) WT ICab3, (**E**) ICab3 V115C, and (**F**) ICab3 H116C. NorC was mixed with WT ICab3 or its mutants in a molar ratio of 1:1. As shown in **D**, arrow indicates decrease in the fluorescence intensity of free ICab3 upon incubation with NorC suggesting its binding with the latter. Also, binding with WT ICab3 results in leftward shift in the elution volume of NorC (also shown in the inset). Corresponding insets in **E** and **F** show affinity of ICab3 V115C and ICab3 H116C towards NorC to be reduced, and abolished, respectively.

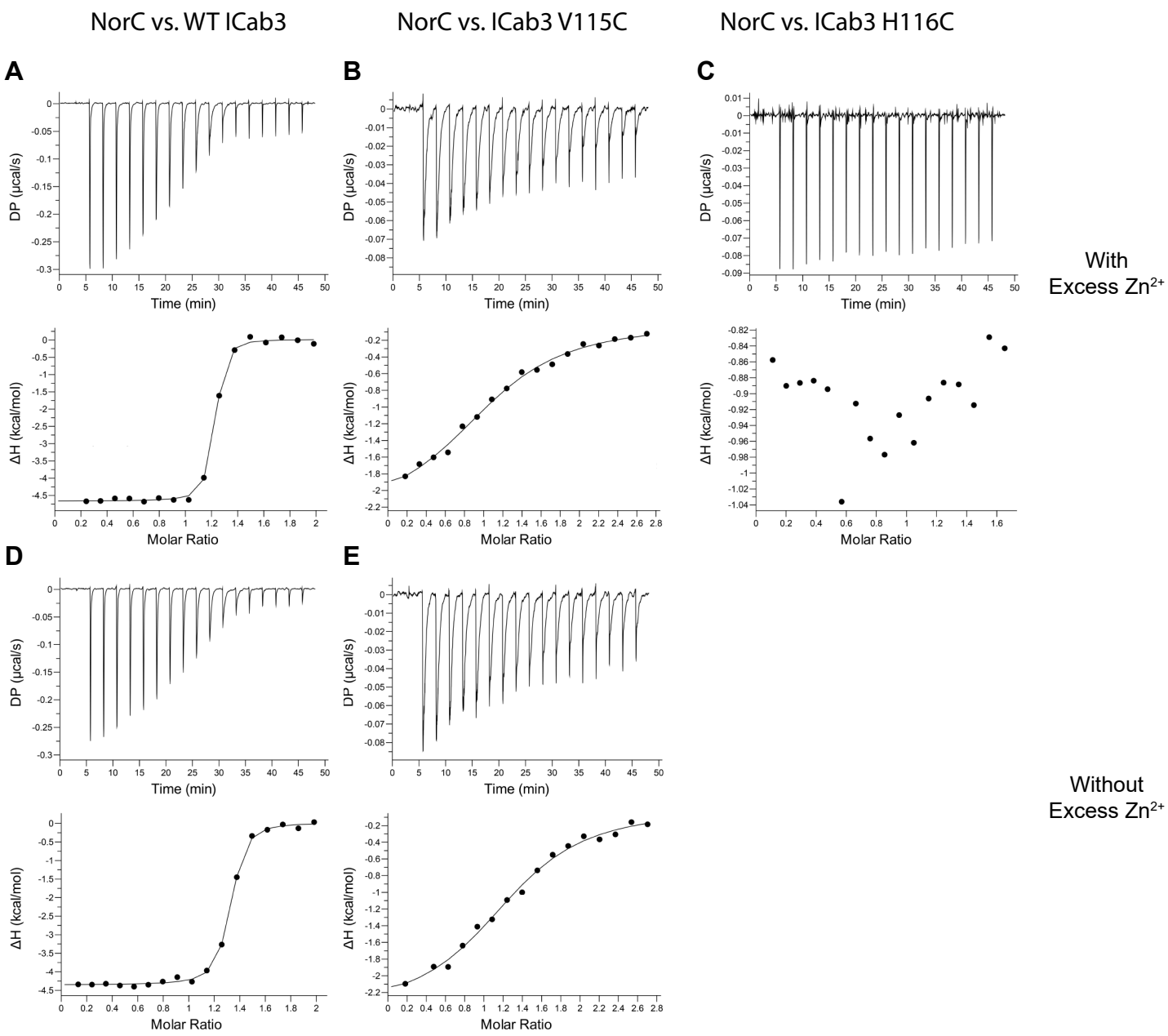

F

	WT ICab3		ICab3 V115C		ICab3 H116C	
	- Zn^{2+}	**+ Zn^{2+}**	**- Zn^{2+}**	**+ Zn^{2+}**	**- Zn^{2+}**	**+ Zn^{2+}**
N (sites)	1.27 ± 0.0	1.17 ± 0.0	1.28 ± 0.05	1.08 ± 0.04	ND	
K_D (nM)	45.2 ± 5.4	19.5 ± 3.8	4071 ± 1040	5690 ± 1430	ND	
ΔH (kcal/mol)	-4.4 ± 0.04	-4.7 ± 0.05	-2.4 ± 0.19	-2.3 ± 0.20	ND	
TΔS (kcal/mol)	5.7	5.8	4.9	4.8	ND	
ΔG (kcal/mol)	-10	-10.5	-7.4	-7.2	ND	
Model	One set of sites	One set of sites	One set of sites	One set of sites	ND	

Figure S7. Binding analysis of ICab3 and its mutants with NorC. ITC profile (differential power, top panel; binding isotherms with integrated peaks normalized to moles of injectant and offset corrected, bottom panel.) showing **A,** nanomolar affinity of WT ICab3 with NorC, **(D)** which increases in the presence of 50 µM Zn^{2+} in the buffer. **B,** The binding affinity decreases 100 fold in case of ICab3 V115C mutant, and is unaffected by the presence of Zn^{2+} **(E)**. **C,** ICab3 H116C has no affinity for NorC even in the presence of excess Zn^{2+}. **F,** The results are summarised in the table.

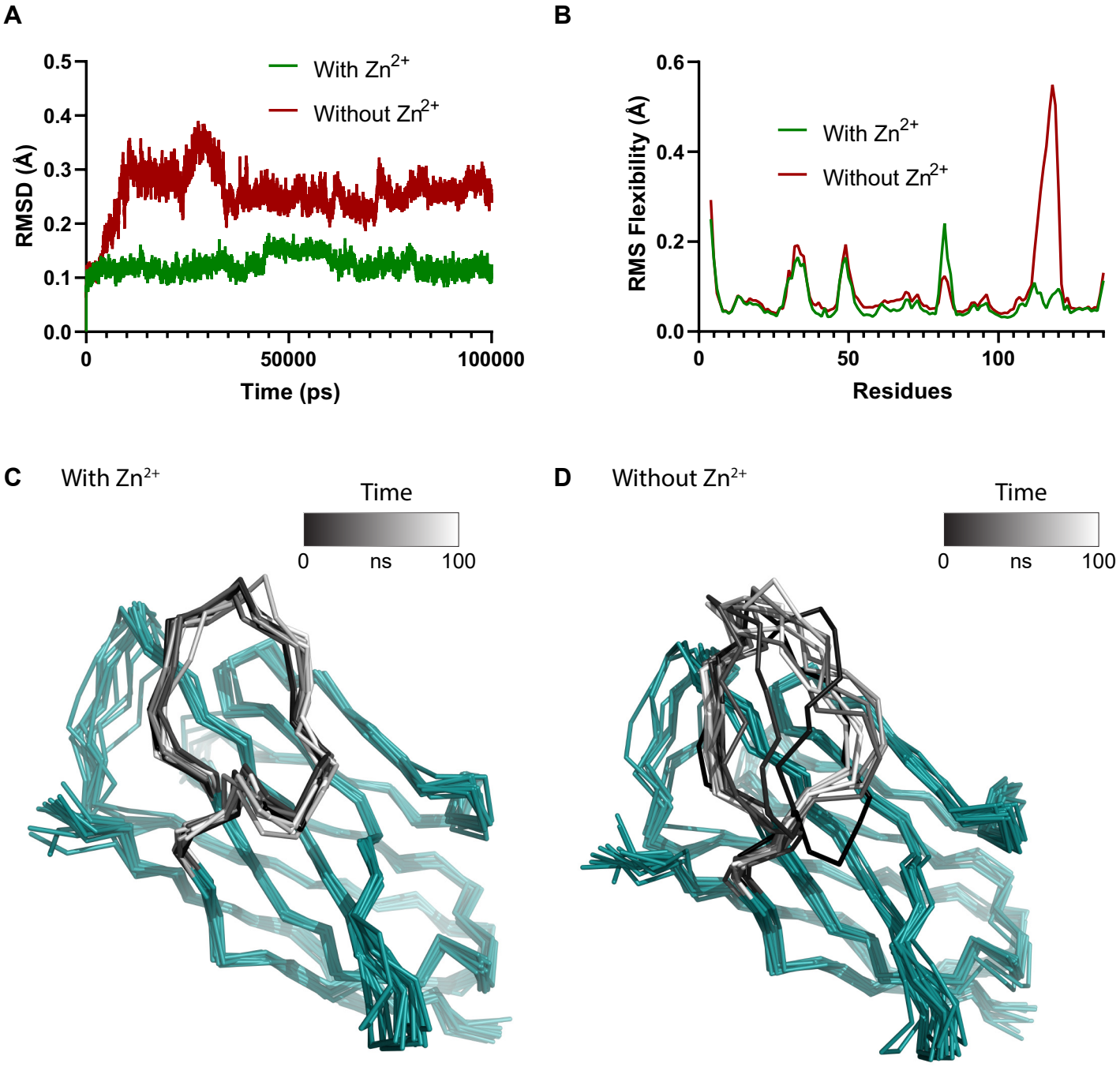

Figure S8. **A**, Plot showing RMSD values of Cα atoms of Zn^{2+}-bound (green) and Zn^{2+}-free (red) WT ICab3 structures obtained from the MD simulation trajectory. **B**, Residue-wise RMS fluctuation of Cα atoms of Zn^{2+}-bound (green) and Zn^{2+}-free (red) WT ICab3 structures suggesting increased fluctuation in CDR3 region upon removal of Zn^{2+}. Superposition of structures of (**C**) Zn^{2+}-bound and (**D**) Zn^{2+}-free WT ICab3 at different time points through the trajectory. As can be seen, only CDR3 region (greyscale) is affected in the absence of Zn^{2+} from the coordination site.